Title

A knockout-first model of H3f3a gene targeting leads to developmental lethality

Journal

Genesis, 61(1-2)

ISSN

1526-954X

Authors

Bush, Kelly
Cervantes, Vanessa
Yee, Jennifer Q
et al.

Publication Date

2023-03-01

DOI

10.1002/dvg.23507

Peer reviewed

HHS Public Access

Author manuscript

Genesis. Author manuscript; available in PMC 2023 March 25.

Published in final edited form as:

Genesis. 2023 March ; 61(1-2): e23507. doi:10.1002/dvg.23507.

A knockout-first model of *H3f3a* gene targeting leads to developmental lethality

Kelly Bush[1,2,3], **Vanessa Cervantes**[1,2,3], **Jennifer Q. Yee**[1,2,3], **Rachel H. Klein**[1,2,3], **Paul S. Knoepfler**[1,2,3]

[1]Department of Cell Biology and Human Anatomy, University of California Davis, Davis, California, USA

[2]Institute for Pediatric Regenerative Medicine, Shriners Hospital for Children Northern California, Sacramento, California, USA

[3]Genome Center, University of California Davis, Davis, California, USA

Summary

Histone variant H3.3 is encoded by two genes, *H3f3a* and *H3f3b*, which can be expressed differentially depending on tissue type. Previous work in our lab has shown that knockout of *H3f3b* causes some neonatal lethality and infertility in mice, and chromosomal defects in mouse embryonic fibroblasts (MEFs). Studies of *H3f3a* and *H3f3b* null mice by others have produced generally similar phenotypes to what we found in our *H3f3b* nulls, but the relative impacts of the loss of either *H3f3a* or *H3f3b* have varied depending on the approach and genetic background. Here we used a knockout-first approach to target the *H3f3a* gene for inactivation in C57BL6 mice. Homozygous *H3f3a* targeting produced a lethal phenotype at or before birth. E13.5 null embryos had some potential morphological differences from WT littermates including smaller size and reduced head size. An E18.5 null embryo was smaller than its control littermates with several potential defects including small head and brain size as well as small lungs, which would be consistent with a late gestation lethal phenotype. Despite a reduction in H3.3 and total H3 protein levels, the only histone H3 post-translational modification in the small panel assessed that was significantly altered was the unique H3.3 mark phospho-Serine31, which was consistently increased in null neurospheres. *H3f3a* null neurospheres also exhibited consistent gene expression changes including in protocadherins. Overall, our findings are consistent with the model that there are differential, cell-type-specific contributions of *H3f3a* and *H3f3b* to H3.3 functions in epigenetic and developmental processes.

Keywords

development; H3f3a; H3f3b; histone H3.3; mouse knockouts; neurospheres

Correspondence: Paul S. Knoepfler, Department of Cell Biology and Human Anatomy, University of California Davis, Davis, CA 95616, USA. knoepfler@ucdavis.edu.

1 | INTRODUCTION

The specific histone molecules making up nucleosomal octamers along with their unique combinations of post-translational modifications (PTMs) are major regulators of chromatin structure and function. Histone H3.3 is a variant member of the histone H3 family that is unusual in a number of ways. Unlike canonical H3 variants H3.1 and H3.2, which are encoded by many genes within gene clusters, H3.3 is encoded by just two separate genes, *H3F3A/H3f3a* and *H3F3B/H3f3b* (in humans and mice, respectively), which differ in chromosomal location and untranslated regions, but encode the identical H3.3 protein (Elsaesser, Goldberg, & Allis, 2010). While the expression of H3.1 and H3.2 largely coincides specifically with S phase, H3.3 is expressed throughout the cell cycle. Fitting with that broader expression pattern, H3.3 is also a replication-independent variant uniquely deposited on chromatin at any phase of the cell cycle (Ahmad & Henikoff, 2002), while the deposition of H3.1 and H3.2 is replication-dependent. H3.3 is thus linked to a broader range of epigenetic functions than H3.1/H3.2, including more dynamic regulation of transcriptional control and facilitation of DNA repair (Luijsterburg et al., 2016).

The H3.3 protein differs from canonical H3.1 by only 5 amino acids, and from H3.2 by 4 amino acids (Elsaesser et al., 2010; Filipescu, Szenker, & Almouzni, 2013), but these differences confer its distinct functions. For example, the unique residues within H3.3 mediate its binding to and deposition by its novel chaperones, HIRA in genic regions, and ATRX/DAXX at regions of heterochromatin including within telomeric regions (Banaszynski et al., 2013; Elsaesser & Allis, 2010; Lewis, Elsaesser, Noh, Stadler, & Allis, 2010), while H3.1/H3.2 have their own distinct chaperones. H3.3 also has somewhat unique patterns of PTMs compared to H3.1/H3.2, and H3.3 tends to be enriched at active chromatin and actively transcribed genes (Ahmad & Henikoff, 2002; McKittrick, Gafken, Ahmad, & Henikoff, 2004). The distinctive localization and functions of H3.3 in centromeric and telomeric regions are likely important as well (Wong et al., 2010).

Phenotypes from *H3f3a* and *H3f3b* loss-of-function studies in mice consistently indicate roles for H3.3 in normal mammalian development (Bush et al., 2013; Couldrey, Carlton, Nolan, Colledge, & Evans, 1999; Jang, Shibata, Starmer, Yee, & Magnuson, 2015; Tang et al., 2015; Tang, Jacobs, Wong, & Mann, 2013; Yuen, Bush, Barrilleaux, Cotterman, & Knoepfler, 2014). The phenotypes associated with the separate single knockouts of *H3f3a* and *H3f3b* have varied in the different published gene targeting studies, likely mainly attributable to differences in both genetic backgrounds and perhaps to some extent to the different methods of gene disruption. However, reduced levels of H3.3 protein have been consistently associated with infertility, genomic instability, and with some degree of embryonic lethality. While *H3f3a* and *H3f3b* encode the same H3.3 protein, there is interest in how the function of these genes may differ. The phenotypes from the aforementioned knockout studies suggest that the relative contributions of *H3f3a* and *H3f3b* to total cellular H3.3 protein levels are in some cases cell-type specific (Bush et al., 2013; Couldrey et al., 1999; Jang et al., 2015; Tang et al., 2013; Tang et al., 2015; Yuen et al., 2014). More specifically, the 2015 data from Tang, et al. suggested a relatively higher contribution of *H3f3a* to H3.3 protein levels in the brain, while we have previously found that *H3f3b* likely contributes more to total H3.3 levels in mouse embryonic fibroblasts (MEFs) and possibly

male germ cells (Bush et al., 2013; Yuen et al., 2014). Even so, notably a more recent gene epitope-tagging study in mice reported that the patterns of relative *H3f3a* and *H3f3b* expression in diverse tissues were remarkably similar overall (Bachu et al., 2019).

Here, we developed a murine model of disrupted *H3f3a* expression in C57BL/6 mice. Applying a knockout-first, conditional-ready targeting approach, disruption of *H3f3a* resulted in developmental lethality, manifesting sometime after mid-gestation to birth. Analyses of both *H3f3a* targeted neurospheres and MEFs indicate a greater contribution of *H3f3a* to H3.3 protein levels in the former and of *H3f3b* in the latter types of cells. We generally did not see compensatory increases in *H3f3b* expression with disruption of *H3f3a* in either cell type. The main histone PTM altered in *H3f3a* deficient cells at a global level in these cells was the H3.3 specific H3.3S31 phosphorylation mark. Overall, these *H3f3a* targeted mice and cells are likely to be useful tools for deciphering this gene's function and advancing knowledge of the functions of the H3.3 protein in normal development and disease.

2 | RESULTS

2.1 | Production of *H3f3a* targeted mice

To determine the functions of the *H3f3a* gene and H3.3 protein in murine development and cell biology, we generated a knock-out first conditional-ready allele (*H3f3a*^{tm1a}; https://www.ncbi.nlm.nih.gov/nucleotide/JN957085.1?report=genbank&log$=nuclalign&blast_rank=1&RID=8ZRU6GXM015) in C57BL/6 N mice using targeted mouse embryonic stem cells (mESCs) available from the Knockout Mouse Project or KOMP Repository (Figure 1a) at the UC Davis Mouse Biology Program (UCD MBP). The rationale for using the knockout-first approach was to efficiently generate data on phenotypes due to *H3f3a* loss-of-function. The knockout-first allele features an in-frame expression cassette (consisting of an *Engrailed2* splice acceptor [En2 SA], lacZ, B-actin promoter, and neomycin) inserted into intron 2 of *H3f3a*, causing a functional gene trap that disrupts *H3f3a* expression. Nearest neighbor protein-coding genes of *H3f3a* (itself located at mm10 chr1:180,800,832–180,813,632) are *Acbd3* (mm10 chr1:180,726,043–180,754,204) >50 kb away, and *Sde2* (mm10 chr1:180,851,127–180,868,113) almost 38 kb away, making any aberrant transcriptional effects on neighboring genes unlikely.

Gene targeting of the *H3f3a*^{tm1a} knockout-first allele in mESC by homologous recombination rather than by random insertion was validated by the UCD MBP via long-range genomic PCR using one primer in the *H3f3a* region but outside the homology arms of the targeting vector paired with an En2 SA primer inside the knockout-first cassette, generating only the expected approximately 2.6 kb product (Figure 1b). The retention and presence of the most distal LoxP site was confirmed by a LoxP PCR assay (Figure 1c).

Germline transmission of *H3f3a*^{tm1a} was attempted via breeding the high-percentage somatic chimera B04, but it failed to be productive (Figure 1d). IVF was conducted using sperm from B04, leading to germline transmission and stable inheritance of the mutant allele. Throughout the study, WT *H3f3a* and knockout-first alleles were detected via gene-

specific genomic PCR and for *H3f3a*^{tm1a} by the presence of the knockout-first cassette (Figure 2a,b).

2.2 | Homozygous lethal and variable heterozygous targeted phenotypes

Numerous *H3f3a*$^{WT/tm1a}$ × *H3f3a*$^{WT/tm1a}$ crosses produced only one surviving homozygous *H3f3a*$^{tm1a/tm1a}$ knockout mouse at birth, indicating a generally lethal phenotype. This surviving knockout appears generally healthy but is infertile. Notably, about half of the *H3f3a*$^{WT/tm1a}$ pups had low body weight (see small heterozygous pup at left in Figure 2c indicated by yellow arrow). This highly variable phenotype in some heterozygous pups included in some cases neonatal lethality, retarded growth, and reduced size, while other heterozygous pups seemed outwardly normal. Despite these partially penetrant initial heterozygous phenotypes, nearly all surviving *H3f3a*$^{WT/tm1a}$ mice eventually grew to normal size and all those that were bred were fertile.

Since there were apparent phenotypic differences between *H3f3a*$^{WT/tm1a}$ pups, as some closely resembled *H3f3a*$^{WT/WT}$ whereas others exhibited early growth retardation or prenatal or neonatal death, we used RT-qPCR to analyze *H3f3a* mRNA expression in surviving *H3f3a*$^{WT/tm1a}$ mice relative to *H3f3a*$^{WT/WT}$ littermates. Approximately half of analyzed *H3f3a*$^{WT/tm1a}$ mice displayed the expected roughly 50% reduction in *H3f3a* expression, while notably, the other half exhibited approximately equal or slightly higher than WT levels of *H3f3a* (Figure 2d). These data suggest that in heterozygotes the *H3f3a*^{tm1a} allele has quite variable rates of transcription, likely correlating with the observed variable heterozygous phenotypes. The one surviving *H3f3a*$^{tm1a/tm1a}$ null mouse exhibited only background levels of *H3f3a* expression relative to WT and heterozygous levels (Figure 2e).

Of the 30 liters analyzed from *H3f3a*$^{WT/tm1a}$ × *H3f3a*$^{WT/tm1a}$ pairs, we observed lower than expected Mendelian ratios of *H3f3a*$^{WT/tm1a}$ mice, which is consistent with some lethality (Table 1). No *H3f3a*$^{tm1a/tm1a}$ pups were found dead at birth or shortly after, consistent with homozygous disruption of *H3f3a* being late embryonic lethal. To further investigate this possibility, we established *H3f3a*$^{WT/tm1a}$× *H3f3a*$^{WT/tm1a}$ timed matings and isolated embryos at 13.5 and 18.5 days post-conception (E13.5 and E18.5).

At E18.5, one null embryo was isolated along with two WT and two heterozygous control littermates. These embryos were embedded, sagittally sectioned, and stained with H&E (Figure 2f). The null was generally smaller than its littermates, and had a small head and brain as well as small lungs. Notably, while the pleural cavities appeared of similar volumes in each E18.5 embryo regardless of genotype, the lungs in the null uniquely fill only a small portion of this cavity.

At E13.5, we observed close-to-expected ratios of *H3f3a*$^{WT/WT}$, *H3f3a*$^{WT/tm1a}$, and *H3f3a*$^{tm1a/tm1a}$ embryos with no underrepresentation of homozygous targeted embryos, suggesting that *H3f3a* null embryos are mostly viable until at least E13.5 (Table 1). The E13.5 *H3f3a*$^{tm1a/tm1a}$ embryos were slightly smaller on average than littermates with small heads that tended to be flatter, consistent with a smaller brain (Figure 3a).

2.3 | Generation of E13.5 targeted cell lines

The same E13.5 embryos as described above were used to generate primary cell lines (Figure 3a). The head was removed to establish neural stem cell and precursor cell lines (neurospheres), internal organs were removed, and the remaining body tissue was used to form lines of MEFs. Despite homozygous disruption of *H3f3a, H3f3a*$^{tm1a/tm1a}$ MEFs and neurospheres generally displayed cellular morphology and growth similar to cells from wildtype littermates (Figure 3b).

To validate the disruption of *H3f3a* expression in *H3f3a*$^{tm1a/tm1a}$ cell lines, we conducted RT-qPCR using Taqman primers specific to *H3f3a*. Only minimal levels of *H3f3a* were detected in *H3f3a*$^{tm1a/tm1a}$ MEFs and neurospheres, likely reflecting background signal (Figure 3c,d). We also analyzed *H3f3b* levels to assess the possibility of compensation in our embryonic cell lines lacking *H3f3a*. While *H3f3b* levels varied between lines for both *H3f3a* null MEFs and neurospheres, on average they displayed levels similar to *H3f3b* expression in control *H3f3a*$^{WT/WT}$ lines (Figure 3e,f), suggesting there are no consistent compensatory increases in *H3f3b* in *H3f3a* null cultured cells.

2.4 | Impact of *H3f3a* knockout on histone H3 marks in primary cells

To examine the effects of *H3f3a* disruption on H3.3 protein levels and potential effects on overall H3 epigenetic marks in a neural precursor context, we performed Western blots on acid histone extracts isolated from neurospheres (Figure 4a,b). Both total H3.3 and H3 protein levels were significantly reduced in *H3f3a*$^{tm1a/tm1a}$ neurospheres relative to control WT cells isolated from the same litters, suggesting a high percentage of total histone H3 is comprised of H3.3 in these cells. Note that the total H3 antibody recognizes all forms of H3 family members including H3.3.

While levels of H3K9 tri-methylation and acetylation remained largely unchanged relative to total H3 levels in null neurospheres as compared to controls, there was an overall two-fold increase in the active mark H3K4me3 in nulls, although not reaching statistical significance. Notably, the H3.3-specific mitotic mark H3.3S31P was elevated in *H3f3a*$^{tm1a/tm1a}$ lines when normalized to H3.3 protein levels (Figure 4a,b).

In parallel, we performed Western blots in control and *H3f3a*$^{tm1a/tm1a}$ MEFs isolated from the same embryos as the neurosphere derivation (Figure 4c,d). Overall, MEFs appeared less affected by the loss of *H3f3a* in terms of histone marks as compared to neurospheres. For instance, while we had seen a marked increase in H3.3S31P levels in *H3f3a*$^{tm1a/tm1a}$ neurospheres, the levels were only slightly elevated in MEFs. Further, although we observed a significant decrease in H3.3 levels in *H3f3a*$^{tm1a/tm1a}$ MEFs, total H3 levels remained relatively unchanged in those cells. Previous studies from our lab suggest that *H3f3b* contributes more to H3.3 protein production in MEFs, which could potentially explain the only moderate epigenetic changes observed here with loss of *H3f3a* (Bush et al., 2013).

2.5 | Analysis of impacts of loss of *H3f3a* on the transcriptome

In order to assess the impact of loss of *H3f3a* on the transcriptome, RNA was isolated from control and knockout neurospheres and MEFs, and analyzed by 3′-Tag-Seq. A small

number of genes were up- or downregulated in null neurospheres (Table 2). As expected, *H3f3a* itself was one of the most strongly downregulated genes in null neurospheres. The expression of several protocadherin genes was significantly changed in the nulls as well. Null MEFs exhibited almost no consistent and significant changes in gene expression, perhaps due to a more dominant role for *H3f3b* in MEFs.

3 | DISCUSSION

In recent years more has been learned about the roles of the H3.3-coding genes *H3f3a* and *H3f3b* in mammalian development. An early gene trap study reported targeting of *H3f3a* led to murine infertility (Couldrey et al., 1999). Single knockouts of the two H3.3 coding genes (*H3.3A* and *H3.3B*) in Drosophila did not strongly affect development and the double *H3.3A/H3.3B* knockout in the fly was compatible with life but led to infertility (Hodl & Basler, 2009; Sakai, Schwartz, Goldstein, & Ahmad, 2009). Single mouse knockout studies have also found that *H3f3a* and *H3f3b* have roles in mammalian fertility and more specifically in gamete and early embryonic states including specifying appropriate chromatin states (Bush et al., 2013; Jang et al., 2015; Tang et al., 2015; Tang, Binos, Ong, Wong, & Mann, 2014; Yuen et al., 2014). Thus, in a broad sense, loss of H3.3 likely leads to infertility due to perturbed chromatin in gametes and early embryos. In mice, double knockout led to a severe, early lethal phenotype and substantial changes in primary H3.3 null cells (Jang et al., 2015).

Our previous work with the *H3f3b* conditional KO system found that some *H3f3b* null mice survive even if they were not fertile (Bush et al., 2013), while in our new studies we found only one surviving *H3f3a* homozygous mutant mouse in years of breeding and found no dead null pups early after birth, most consistent with a late embryonic lethal phenotype. This pattern of *H3f3a* and *H3f3b* phenotypes is generally the opposite of that observed by the Mann group, where they found more severe effects of loss of *H3f3b* versus *H3f3a* (Tang et al., 2014; Tang et al., 2015). One potentially straightforward explanation for these differences is the distinct genetic backgrounds of the mice in these studies (C57BL/6 in our work versus 129 or 129 mixed with C57BL/6 in mice from the other labs). Furthermore, given that different methods were used for gene targeting, such technological differences may contribute to different phenotypes reported by the various labs as well. More specifically, while we used a knockout-first gene trapping approach for disruption of *H3f3a*, other labs deleted exonic portions of the gene.

We also observed that some heterozygously targeted *H3f3a* mice exhibited only temporary impaired growth phenotypes early on. The variably reduced *H3f3a* expression in our $H3f3a^{WT/tm1a}$ mice likely explains part of their variable phenotype. It is also possible that in $H3f3a^{WT/tm1a}$ mice that the targeted allele is sometimes expressed at low but sufficient levels to avoid an obvious phenotype.

Transient and variable phenotypes with homozygous loss of one of the two H3.3-coding genes could be due to variable compensation by the remaining H3.3-coding gene or other compensatory mechanisms in cells and organisms such as changes in H3.3 chaperone function. In fully H3.3 deficient, double knockout flies, canonical H3 was also reported

to have elevated expression and begin functioning in a partially replication-independent manner compensating for loss of H3.3 (Sakai et al., 2009), perhaps explaining the mechanism by which some double knockouts could survive. It is unknown whether loss of H3.3 induces H3.1 or H3.2 to function in a more H3.3-like manner in mammals, but that also could contribute to variability in knockout phenotypes.

In humans, mutations in *H3F3A* and *H3F3B* are associated with different kinds of tumors, which may in part reflect their differences in expression patterns. *H3F3A* mutations are commonly found in high-grade childhood gliomas (reviewed in [Yuen & Knoepfler, 2013]), fitting with a proposed role for *H3F3A* expression more strongly contributing to H3.3 protein levels in the brain, while *H3F3B* mutations are by contrast most often present in childhood bone and cartilage tumors (Behjati et al., 2013). Although the specific molecular roles of distinct mutant H3.3 proteins in these tumors are not fully understood, the findings so far support a model in which key normal epigenetic functions of H3.3 in neurodevelopmental programs are perturbed by each of the tumor-associated H3.3 mutant proteins, with some overlap in H3.3 K27M and G34R mutation mechanisms (Chen et al., 2020). This model is consistent with the murine loss-of-function studies pointing to H3.3 epigenetic regulation of normal development via impact on gene expression. In glioma, mutant H3.3 is also associated with perturbed Polycomb repressive complex 2 (PRC2) activity and aberrant patterns of histone modifications including in particular H3K27me3 (Jain et al., 2020). It is unclear if H3.3 normally functions broadly in the developing embryo in part via PRC2 specifically in stem cells but work in mESC indicating a central role for HIRA-H3.3 in PRC2 function (Banaszynski et al., 2013) makes this likely.

More recent work has identified distinct mutations in *H3F3A* and *H3F3B* in people with neurodevelopmental disorders as well, pointing to specific nervous system functions (Bryant et al., 2020). Our analysis of the *H3f3a* null E18.5 embryo suggested a small brain phenotype, which could be consistent with the mutant phenotypes in humans and warrants further exploration. The small lungs in the *H3f3a* null E18.5 embryo are potentially consistent with findings from H3.3-coding gene knockouts from others who reported finding targeted animals with respiratory problems (Jang et al., 2015).

We found that loss of *H3f3a* and the accompanying decrease in H3.3 protein levels had moderate effects on epigenetic marks in MEFs or neurospheres. The most pronounced change was an increase in the H3.3-specific mark H3.3S31P in null neurospheres and our previous work found changes in this mark in *H3f3b* null MEFs (Bush et al., 2013) as well. Effects on histone marks of partial loss of H3.3 by targeting either *H3f3a* or *H3f3b* appear to be highly cell-type dependent.

Loss of *H3f3a* also only had modest effects on the transcriptome. Few effects were found in null MEFs, while null neurospheres exhibited relatively more changes, but still only moderate overall. Only moderate changes in the transcriptome with loss of H3.3-coding genes has been reported before (Jang et al., 2015), suggesting the presence of compensatory or redundant mechanisms. It is also possible that the primary normal function of H3.3 is not to regulate the transcriptome.

Overall, additional genetic tools for studying *H3f3a*, *H3f3b*, and H3.3 will shed more light on their functions in normal development and in diseases such as childhood cancer and neurodevelopmental disorders.

4 | METHODS

4.1 | Data sharing

The Tag-Seq data from our neurosphere analysis has GEO accession number GSE216047.

4.1.1 | Transgenic H3f3a knockout-first mouse production—Details of the production of targeted mice are described in the Results section. While the mice were originally generated as C57BL6/N they were also at some point bred with C57BL6/J leading to a mixed C57BL6 background. Long-range PCR for genotyping mESCs and mice to determine homologous versus non-homologous recombination was conducted using the following primers:

CSD-en2frt-R 5′-GGTGGTGTGGGAAAGGGTTCGAAG-3′.

CSD-H3f3a-LF1 5′-TCCTCTTTCTTCGGTGAAATCCCTCC-3′.

The LoxP PCR assay used the following primers:

CSD-H3f3a-SR1 5′-AGAAACAGCTCAACCAATCACACACC-3′.

CSD-loxPcomF 5′-GAGATGGCGCAACGCAATTAAT-3′.

4.1.2 | Genotyping—All genotyping was performed using Bioneer AccuPower pre-mixed tubes (http://www.bioneer.com) and primers targeting LacZ for the transgenic allele, and regions 5′ and 3′ to the transgenic insertion site for WT. The amplicon sizes are 228 bp and 389 bp for WT and transgenic, respectively. See Figures 1a–c and 2a–b for details.

WT F: 5′-TGG GGA GCA GAA ATT TTT TTT ATT A-3′.

WT R: 5′-CTT CTA AAC ATA CAA AAC GTG GG-3′.

LacZ F: 5′-GTT GCA GTG CAC GGC AGA TAC ACT TGC TGA-3′.

LacZ R: 5′-GCC ACT GGT GTG GGC CAT AAT TCA ATT CGC-3′.

4.1.3 | Creation of primary cell lines—$H3f3a^{WT/tm1a}$ × $H3f3a^{WT/tm1a}$ crosses were time mated, and upon observance of a plug, embryos were isolated at E13.5. The visceral tissue was removed and used for genotyping, while the head region was used to establish the neurosphere lines as described (Knoepfler et al., 2006), and the body was used to produce MEFs. Neurospheres were initially cultured on low-bind plates (Corning; 3261) in N+ media (Neurobasal media, 1x B27, 1% Pen/Strep/Glutamine), bFGF (20 ng/ml), EGF (20 ng/ml) and cultured routinely in low-bind dishes or suspension flasks (Olympus Plastics; 25–213). MEFs were cultured in DMEM enriched with 10% FBS, 1% non-essential amino acids, and 1% Glutamine. All cells were incubated at 37°C with 5% CO_2.

4.1.4 | RNA and cDNA production and qPCR—RNA was extracted from primary cell cultures or tail tips using the NucleoSpin RNA kit produced by Macherey-Nagel

(Macherey-Nagel; 740955.50). 1 μg of RNA was transcribed into cDNA using an iScript cDNA synthesis kit (Bio-Rad; 1708891). cDNA was further diluted and used in qPCR experiments.

qPCR for *H3f3a, H3f3b* and house-keeping control *Eif4g2* was performed using Taqman probes (Applied biosystems; mm01612808_g1, mm00787223_s1 and mm00469036_m1, respectively) and associated protocol. All other genes were analyzed using Sybr Blue master-mix (Abgene; AB4162) or PowerUp SYBR mix (Thermo; A25741) with primers designed in lab. 96-well plates were run on Roche Light Cycler 480, and results were analyzed statistically using the $2^{-\delta\delta Ct}$ method.

4.1.5 | Protein analysis—Histone extracts were prepared from *H3f3a* MEFs and neurospheres using the Abcam protocol with a few modifications. Briefly, cells were washed in PBS with 5 mM Sodium Butyrate, and lysed in TBE buffer (0.5% Triton X-100, 0.02% sodium azide plus Protease inhibitor: Roche; 11836170001). Cells were then pelleted, re-suspended in 0.2 N HCl, and rocked overnight at 4°C. Supernatant was neutralized using 1 N NaOH and frozen at 80°C. Samples were processed with LDS sample buffer (Life Technologies; NP0008) and DTT and run on 6–12% Bis-Tris SDS Nupage gels (Life Technologies; *NP0335BOX*). Proteins were then transferred onto PVDF membranes and probed with the antibodies (Table 3). Results were normalized to actin for H3/H3.3 and histone-marks were normalized to actin and H3 or H3.3. For statistical analysis, *p*-values were calculated using an unpaired *t* test.

4.2 | Tag-Seq (RNA-Seq) analysis

RNA was extracted from WT and KO cells using the NucleoSpin RNA Kit (Macherey-Nagel). Samples were submitted to UC Davis Genome Center DNA Technologies Core where RNA quality was assessed by Agilent Bioanalyzer and libraries were prepared using QuantSeq 3′ mRNA-Seq Library Prep Kit FWD for Illumina. Sequencing was performed on three biological replicates each for WT MEFs, WT neurospheres, and KO neurospheres and five biological replicates for KO MEFs on Illumina HiSeq 4,000. Transcript abundance was quantified by Salmon (version 1.1.0) based on the ensemble-release87 (Mus_musculus.GRCm38.cdna.all.fa) and imported by Tximport (Bioconductor version 3.10). Downstream differential expression was then determined by EdgeR (Bioconductor version 3.10). Data was subject to a threshold of FDR <0.05 and *p*-value ≤.01. Raw and analyzed 3′-Tag-seq data are accessible via GEO.

ACKNOWLEDGMENTS

This work was supported by the following NIH grants to Paul S. Knoepfler: 1R01GM116919 and 1R01NS106878. We want to thank the University of California, Davis Mouse Biology Program for their help with the generation and analysis of the mice. We thank Kent Lloyd and Louise Lanoue for providing feedback on the manuscript and data.

Funding information

National Institute of General Medical Sciences, Grant/Award Number: 1R01GM116919; National Institute of Neurological Disorders and Stroke, Grant/Award Number: 1R01NS106878

DATA AVAILABILITY STATEMENT

GEO accession number is GSE216047.

REFERENCES

Ahmad K, & Henikoff S (2002). The histone variant H3.3 marks active chromatin by replication-independent nucleosome assembly. Molecular Cell, 9(6), 1191–1200 http://www.ncbi.nlm.nih.gov/entrez/query.fcgi?cmd=Retrieve&db=PubMed&dopt=Citation&list_uids=12086617 [PubMed: 12086617]

Bachu M, Tamura T, Chen C, Narain A, Nehru V, Sarai N, … Ozato K (2019). A versatile mouse model of epitope-tagged histone H3.3 to study epigenome dynamics. Journal of Biological Chemistry, 294(6), 1904–1914. 10.1074/jbc.RA118.005550 [PubMed: 30552116]

Banaszynski LA, Wen D, Dewell S, Whitcomb SJ, Lin M, Diaz N, … Allis CD (2013). Hira-dependent histone H3.3 deposition facilitates PRC2 recruitment at developmental loci in ES cells. Cell, 155(1), 107–120. 10.1016/j.cell.2013.08.061 [PubMed: 24074864]

Behjati S, Tarpey PS, Presneau N, Scheipl S, Pillay N, Van Loo P, … Flanagan AM (2013). Distinct H3F3A and H3F3B driver mutations define chondroblastoma and giant cell tumor of bone. Nature Genetics, 45(12), 1479–1482. 10.1038/ng.2814 [PubMed: 24162739]

Bryant L, Li D, Cox SG, Marchione D, Joiner EF, Wilson K, … Bhoj EJ (2020). Histone H3.3 beyond cancer: Germline mutations in histone 3 family 3A and 3B cause a previously unidentified neurodegenerative disorder in 46 patients. Science Advances, 6(49), eabc9207. 10.1126/sciadv.abc9207 [PubMed: 33268356]

Bush KM, Yuen BT, Barrilleaux BL, Riggs JW, O'Geen H, Cotterman RF, & Knoepfler PS (2013). Endogenous mammalian histone H3.3 exhibits chromatin-related functions during development. Epigenetics & Chromatin, 6(1), 7. 10.1186/1756-8935-6-7 [PubMed: 23570311]

Chen KY, Bush K, Klein RH, Cervantes V, Lewis N, Naqvi A, … Knoepfler PS (2020). Reciprocal H3.3 gene editing identifies K27M and G34R mechanisms in pediatric glioma including NOTCH signaling. Communications Biology, 3(1), 363. 10.1038/s42003-020-1076-0 [PubMed: 32647372]

Couldrey C, Carlton MB, Nolan PM, Colledge WH, & Evans MJ (1999). A retroviral gene trap insertion into the histone 3.3A gene causes partial neonatal lethality, stunted growth, neuromuscular deficits and male sub-fertility in transgenic mice. Human Molecular Genetics, 8(13), 2489–2495 https://www.ncbi.nlm.nih.gov/pubmed/10556297 [PubMed: 10556297]

Elsaesser SJ, & Allis CD (2010). HIRA and Daxx constitute two independent histone H3.3-containing predeposition complexes. Cold Spring Harbor Symposia on Quantitative Biology, 75, 27–34. 10.1101/sqb.2010.75.008 [PubMed: 21047901]

Elsaesser SJ, Goldberg AD, & Allis CD (2010). New functions for an old variant: no substitute for histone H3.3. Current Opinion in Genetics and Development, 20(2), 110–117. 10.1016/j.gde.2010.01.003 [PubMed: 20153629]

Filipescu D, Szenker E, & Almouzni G (2013). Developmental roles of histone H3 variants and their chaperones. Trends in Genetics, 29(11), 630–640. 10.1016/j.tig.2013.06.002 [PubMed: 23830582]

Hodl M, & Basler K (2009). Transcription in the absence of histone H3.3. Current Biology, 19(14), 1221–1226. 10.1016/j.cub.2009.05.048 [PubMed: 19523831]

Jain SU, Khazaei S, Marchione DM, Lundgren SM, Wang X, Weinberg DN, … Lewis PW (2020). Histone H3.3 G34 mutations promote aberrant PRC2 activity and drive tumor progression. Proceedings of the National Academy of Sciences of the United States of America, 117(44), 27354–27364. 10.1073/pnas.2006076117 [PubMed: 33067396]

Jang CW, Shibata Y, Starmer J, Yee D, & Magnuson T (2015). Histone H3.3 maintains genome integrity during mammalian development. Genes and Development, 29(13), 1377–1392. 10.1101/gad.264150.115 [PubMed: 26159997]

Knoepfler PS, Zhang XY, Cheng PF, Gafken PR, McMahon SB, & Eisenman RN (2006). Myc influences global chromatin structure. EMBO Journal, 25(12), 2723–2734 http://www.ncbi.nlm.nih.gov/entrez/query.fcgi?cmd=Retrieve&db=PubMed&dopt=Citation&list_uids=16724113 [PubMed: 16724113]

Lewis PW, Elsaesser SJ, Noh KM, Stadler SC, & Allis CD (2010). Daxx is an H3.3-specific histone chaperone and cooperates with ATRX in replication-independent chromatin assembly at telomeres. Proceedings of the National Academy of Sciences of the United States of America, 107(32), 14075–14080. 10.1073/pnas.1008850107 [PubMed: 20651253]

Luijsterburg MS, de Krijger I, Wiegant WW, Shah RG, Smeenk G, de Groot AJL, … van Attikum H (2016). PARP1 links CHD2-mediated chromatin expansion and H3.3 deposition to DNA repair by non-homologous end-joining. Molecular Cell, 61(4), 547–562. 10.1016/j.molcel.2016.01.019 [PubMed: 26895424]

McKittrick E, Gafken PR, Ahmad K, & Henikoff S (2004). Histone H3.3 is enriched in covalent modifications associated with active chromatin. Proceedings of the National Academy of Sciences of the United States of America, 101(6), 1525–1530 http://www.ncbi.nlm.nih.gov/entrez/query.fcgi?cmd=Retrieve&db=PubMed&dopt=Citation&list_uids=14732680 [PubMed: 14732680]

Sakai A, Schwartz BE, Goldstein S, & Ahmad K (2009). Transcriptional and developmental functions of the H3.3 histone variant in drosophila. Current Biology, 19(21), 1816–1820. 10.1016/j.cub.2009.09.021 [PubMed: 19781938]

Tang MC, Binos S, Ong EK, Wong LH, & Mann JR (2014). High histone variant H3.3 content in mouse prospermatogonia suggests a role in epigenetic reformatting. Chromosoma, 123(6), 587–595. 10.1007/s00412-014-0475-8 [PubMed: 25007861]

Tang MC, Jacobs SA, Mattiske DM, Soh YM, Graham AN, Tran A, … Mann JR (2015). Contribution of the two genes encoding histone variant h3.3 to viability and fertility in mice. PLoS Genetics, 11(2), e1004964. 10.1371/journal.pgen.1004964 [PubMed: 25675407]

Tang MC, Jacobs SA, Wong LH, & Mann JR (2013). Conditional allelic replacement applied to genes encoding the histone variant H3.3 in the mouse. Genesis, 51(2), 142–146. 10.1002/dvg.22366 [PubMed: 23315948]

Wong LH, McGhie JD, Sim M, Anderson MA, Ahn S, Hannan RD, … Choo KH (2010). ATRX interacts with H3.3 in maintaining telomere structural integrity in pluripotent embryonic stem cells. Genome Research, 20(3), 351–360. 10.1101/gr.101477.109 [PubMed: 20110566]

Yuen BT, Bush KM, Barrilleaux BL, Cotterman R, & Knoepfler PS (2014). Histone H3.3 regulates dynamic chromatin states during spermatogenesis. Development, 141(18), 3483–3494. 10.1242/dev.106450 [PubMed: 25142466]

Yuen BT, & Knoepfler PS (2013). Histone H3.3 mutations: A variant path to cancer. Cancer Cell, 24(5), 567–574. 10.1016/j.ccr.2013.09.015 [PubMed: 24229707]

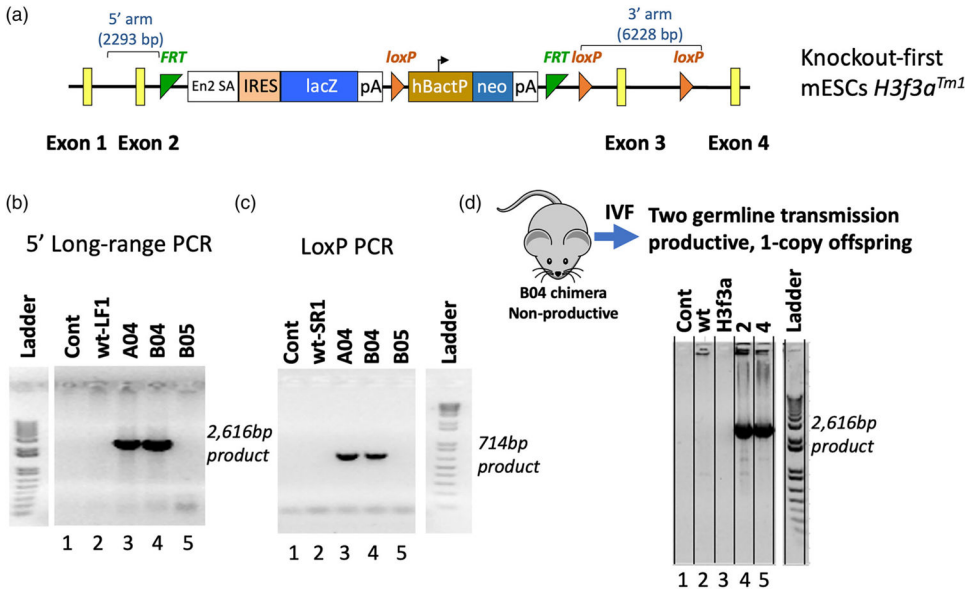

FIGURE 1.

Production and validation of the *H3f3a* targeted mice. A knock-out first conditional-ready allele (*H3f3a*^{tm1a}) was generated in C57BL/6 N mice using targeted mouse embryonic stem cells (mESCs) from the KOMP Repository. (a) Map of the targeted allele. (b) and (c) Long-range and Lox-specific genomic PCR validation assays, respectively. Gene targeting of the *H3f3a*^{tm1a} allele in mESC by homologous recombination rather than by random insertion was validated via long-range genomic PCR using one primer in the *H3f3a* region but outside the homology arms of the targeting vector paired with an En2 SA primer inside the knockout-first cassette, producing the specific approximately 2.6 kb product. The retention and presence of the most distal LoxP site was confirmed by the LoxP PCR assay. (d) After IVF, the correct *H3f3a*^{tm1a} allele was detected in offspring. Data in panels b-d are from the UC Davis Mouse Biology Program as they validated the *H3f3a* targeted ES cells and mice. Because they run a variety of samples from different projects on the same gels, the data not relevant to this project were cropped out. We have included the ladder from the same gel in each case but only with the data relevant to the *H3f3a* project. Areas of cropping are indicated by white gaps between lanes. The Controls “Cont” in b-d contain no template negative controls, and in each case lane 2 is another negative control

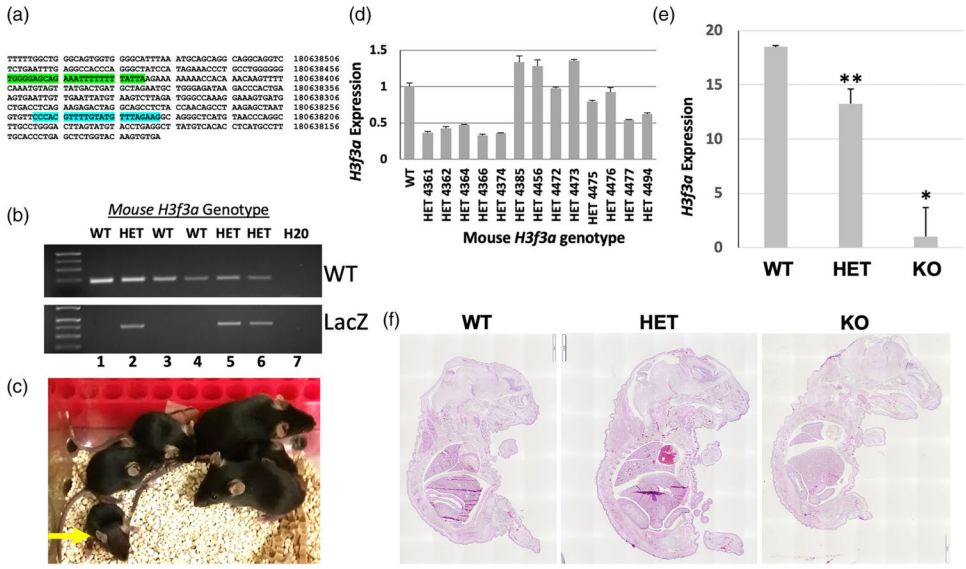

FIGURE 2.

Phenotypes of *H3f3a* targeted mice and evidence of embryonic lethality. (a) Sequence of the WT *H3f3a* allele with WT genotyping primer binding sites highlighted from UCSC Browser (mm39). (b) Example of WT and knockout-first allele (LacZ) amplicons detected via gene-specific genomic PCR. (c) A representative litter of pups generated from heterozygous crosses. All surviving pups were WT or heterozygous. A small heterozygous pup at the left is indicated by the yellow arrow. (d) *H3f3a* RNA levels by RT-qPCR in WT and heterozygous pups; heterozygous *H3f3a* RNA levels are heterogeneous. (e) *H3f3a* RNA levels in WT, heterozygous, and null animal ear tissue samples. (f) Representative H&E stained sections of E18.5 littermate embryos from heterozygous intercrosses are shown. Error bars are the standard deviation of triplicate samples in (d–e) and *p* values for WT versus heterozygous and null are = .0002 and .002, respectively for ** and *

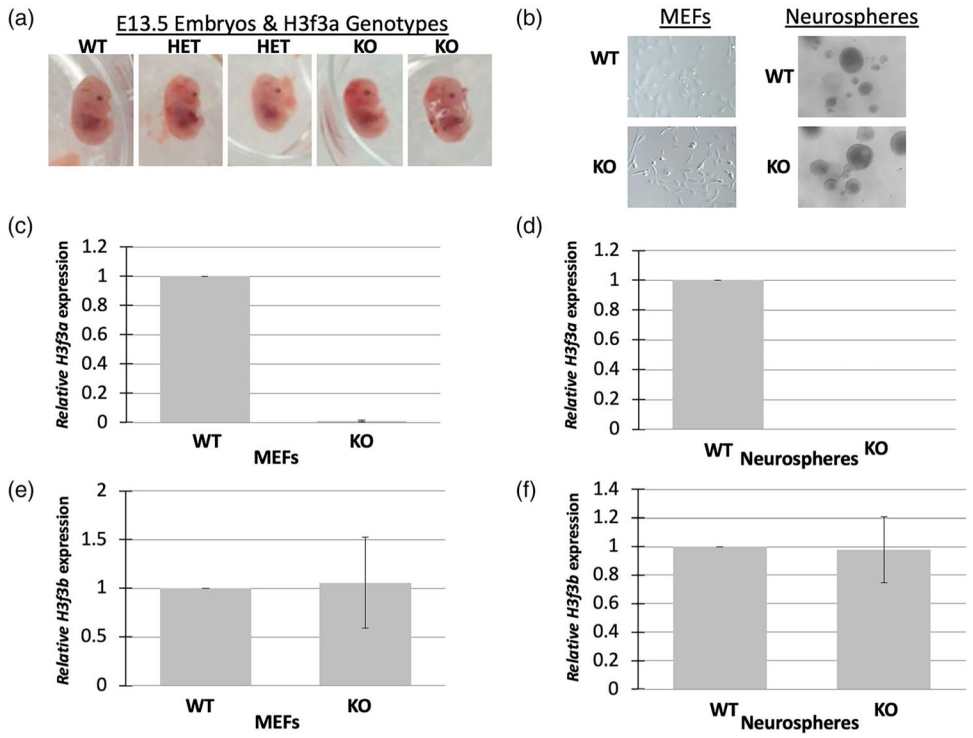

FIGURE 3.

H3f3a targeted MEFs and neurospheres. (a) Heterozygous and null mid-gestational embryos exhibit aberrant phenotypes including small heads. Timed matings were conducted and E13.5 embryos were isolated from heterozygous crosses. Representative embryos are shown. (b) MEFs and neurospheres were isolated from the embryos and cultures established. There were no obvious phenotypes of the cells of different genotypes. (c–d) *H3f3a* null MEFs and neurospheres exhibited nearly undetectable levels of *H3f3a* RNA, and (e–f) no significant changes in *H3f3b* RNA. MEFs and neurospheres were produced from one WT, two heterozygous, and two null embryos for RNA analysis

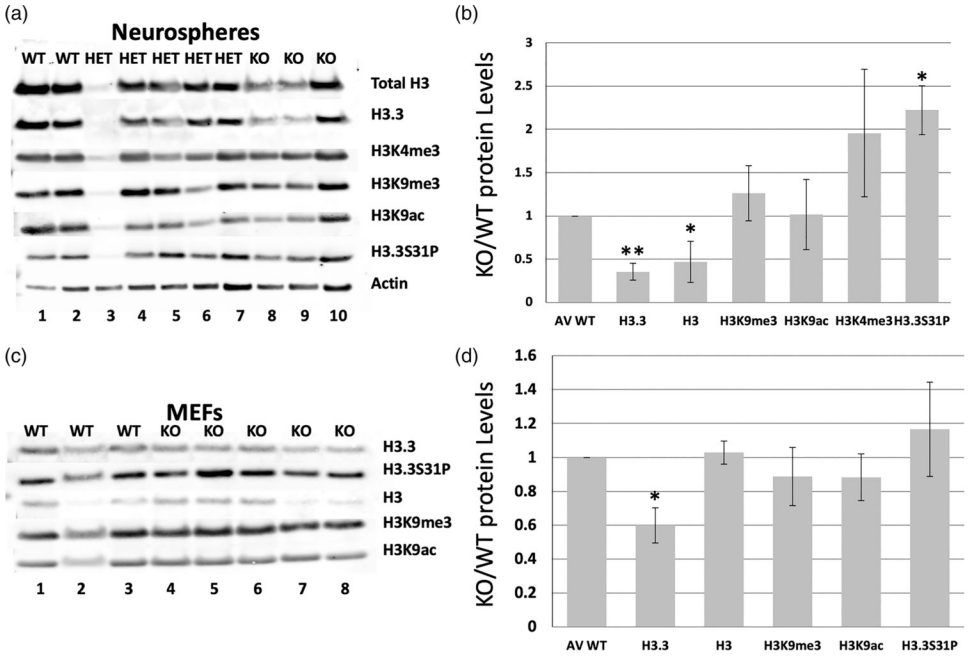

FIGURE 4.

Loss of *H3f3a* strongly reduces both total H3 and H3.3 protein levels, but only impacts some histone H3 family marks. Histone extracts were isolated from *H3f3a* null MEFs and neurospheres, and analyzed by Western blot for total H3, H3.3, and a panel of histone marks. (a–b) Western blots for the indicated histone marks and controls of total H3, total H3.3, and b-Actin levels in neurospheres. (c–d) Western blots for the indicated histone marks and controls of total H3, total H3.3, and b-Actin levels in MEFs. Error bars are standard deviations. *P* values are <.05 and <.005 for * and ** marked samples. MEFs and neurospheres were derived from two WT, five heterozygous, and three null embryos here for histone mark protein level analysis

TABLE 1

H3f3a knockout-first mice are underrepresented from heterozygous intercrosses after E13.5

	H3f3a$^{WT/WT}$	**H3f3a$^{WT/t}$**	**H3f3a$^{t/t}$**
>p21 (30)	46	63	1
Ratio	0.42	0.57	0.01
E18.5 (2)	2	5	1
Ratio	0.25	0.63	0.13
E13.5 (3)	3	9	5
Ratio	0.18	0.53	0.29

TABLE 2

Genes with the most significantly altered expression from Tag-Seq analysis of *H3f3a* knockout neurospheres versus wild-type neurospheres. *H3f3a* itself, bolded in the table, was the gene with the second biggest drop in expression

Official gene symbol or designation	logFC	*p* value	FDR
ENSMUST00000080170	−6.6280	2.38 E-06	0.0175
h3f3a	**6.5807**	**3.43 E-06**	**0.0219**
hmcn1	−5.0349	1.16 E-11	3.70 E-07
fras1	−4.0930	5.56 E-17	2.66 E-12
tusc1	−3.8684	2.25 E-07	0.0027
irs4	−3.8113	2.00 E-06	0.0159
pcdhga3	−3.2228	3.83 E-09	7.34 E-05
slc6a11	1.2595	5.26 E-06	0.0296
pcdhb7	2.4457	1.21 E-07	0.0019
gsta4	2.5102	2.75 E-06	0.0188
cd38	3.2081	2.01 E-10	4.81 E-06
kcnk1	3.2697	1.47 E-06	0.0145
g530011o06rik	3.5724	1.67 E-07	0.0022
nrn1	5.2609	2.34 E-18	2.24 E-13
pcdh15	6.5435	4.40 E-06	0.0263
gmll549	6.6440	1.67 E-06	0.01456
trim30d	7.2172	1.63 E-06	0.01456

TABLE 3

Antibodies used

Target	Vendor	Cat #	Dilution
Total H3	Millipore	05–499	1:2,000
H3.3	Abnova	H00003021-M01	1:2,500
H3.3	Millipore	09–838	1:1,000
H3K4me3	Millipore	07–523	1:2,000
H3K9me3	Millipore	04–745	1:3,000
H3K9ac	Abcam	ab12179	1:2,000
H3.3S31P	Abcam	ab92628	1:1,000
B-Actin	Sigma	A1978	1:5,000